

Ice CO-ictails in molecular cloud cores

T.C. Teixeira¹, J.P. Emerson¹, and M.E. Palumbo²

¹ Department of Physics, Queen Mary and Westfield College, Mile End Road, London E1 4NS, UK
(t.c.teixeira@qmw.ac.uk and j.p.emerson@qmw.ac.uk)

² Osservatorio Astrofisico di Catania, V.le A. Doria 6, I-95125 Catania, Italy (mepalumbo@alpha4.ct.astro.it)

Received 3 September 1996 / Accepted 16 September 1997

Abstract. Spectra of the $4.67\ \mu\text{m}$ ($2140\ \text{cm}^{-1}$) solid-CO absorption feature are presented, towards embedded low mass Young Stellar Objects in nearby molecular cloud cores, mostly in Taurus. The likely composition of the CO-bearing ices is analysed by fitting the observations with laboratory data and the statistical significance of the results is discussed. Excellent fits to the nonpolar component of the CO-ices along the observed lines of sight are produced with irradiated pure CO ices, as previously suggested by Palumbo & Strazzulla (1993). It does not seem to be possible, however, to constrain the composition of the polar component by analysis of the CO band only. The possible origin of the ion irradiation is discussed. The implications of the non-uniqueness of the fit on the determination of the abundance ratio between nonpolar and polar CO-ices are noted. Future observations are suggested to discriminate between the different possibilities for the polar component. Predictions are made for the abundance of CO₂ and methanol in the mantles.

Key words: circumstellar matter – stars: formation – stars: pre-main sequence – ISM: dust, extinction, – ISM: molecules – infrared: ISM: lines and bands

1. Introduction

The study of the composition of the icy mantles that form on dust grains in certain regions of the interstellar medium, including star forming molecular cloud cores, is important for trying to understand the role of such mantles in the chemistry of the interstellar medium, and in understanding the abundances of gaseous species that may freeze out onto the grains, as well as in understanding the optical properties of the grains for input into radiative transfer models. We report observations of the solid CO absorption feature at $4.67\ \mu\text{m}$ and their interpretation in terms of the nature of the ices making up the grain mantles.

Spectroscopic studies of nearby molecular clouds have established the presence of complex icy mantles on the dust grains

in these regions. A variety of absorption bands in infrared spectra of objects in or behind the clouds have been identified as the vibrational transitions of the molecules in the ices (Whittet 1993). Water-ice has been found to be the most abundant component of the ice mantles (Whittet et al. 1988, Eiroa & Hodapp 1989, Tanaka et al. 1990, Tanaka et al. 1994). With an abundance of 10 – 40% relative to the water-ice, CO has also been observed to be an important constituent of the ices (Tielens et al. 1991, Kerr et al. 1993, Tanaka et al. 1994, Chiar et al. 1994, 1995). The presence of CO₂ in significant amounts in the grain mantles, originally reported by d’Hendecourt & de Muizon (1989), has now been confirmed by ISO, reaching 10 – 20% of the abundance of solid-H₂O (e.g. de Graauw et al. 1996, Gürtler et al. 1996). Methanol (CH₃OH) has also been found to be abundant in the ice mantles towards some lines of sight (Grim et al. 1991, Allamandola et al. 1992, Skinner et al. 1992, Tielens & Allamandola 1987, Schutte et al. 1996), but absent towards the Taurus molecular cloud (Chiar et al. 1996), although its overall abundance in the ices remains uncertain. Other molecules have also been detected as more minor constituents of the interstellar ices, but are not of relevance here. A recent review on the formation and evolution of the ice mantles can be found in Schutte (1996).

CO is the most volatile of the main species observed in grain mantles. When dominant in a mantle, CO can only survive sublimation for temperatures below $\sim 17\ \text{K}$, but it can remain in the ices at higher temperatures when trapped in less volatile matrices (e.g. H₂O). Observations of solid CO towards protostellar cores can thus provide a valuable insight on the physical and chemical conditions in the coolest, outer parts of a protostellar envelope (and perhaps in dense circumstellar discs). The field was recently reviewed by Whittet & Duley (1991).

Solid CO in grain mantles can be identified by an absorption band at $4.67\ \mu\text{m}$ ($2140\ \text{cm}^{-1}$), corresponding to the fundamental stretching vibration of the molecule. Laboratory studies have shown that the profile (peak position, width and shape) of the band is sensitive to the composition, structure and thermal and irradiation history of the ices containing the CO (Sandford et al. 1988, Schmitt et al. 1989, Palumbo & Strazzulla 1993, Leto et al. 1996). The comparison of the CO-ice bands observed towards

astronomical objects with laboratory astrophysical analogs can therefore be a powerful probe of the astrophysical environment where those mantles exist, and of the history of the grains (e.g. Tielens et al. 1991, Chiar et al. 1995).

Observations of the CO feature towards varied lines of sight, mostly towards field stars or towards high mass YSOs, have shown that its profile varies from source to source. However, in most cases the feature consists of two distinct components: a sharper dominant absorption at $\sim 4.674 \mu\text{m}$ ($\sim 2140 \text{ cm}^{-1}$), and an overlapping broader and generally weaker one at $\sim 4.681 \mu\text{m}$ ($\sim 2136 \text{ cm}^{-1}$) appearing as a long-wavelength wing (Tielens et al. 1991, Kerr et al. 1993, Chiar et al. 1994, 1995). These authors have attempted to determine the likely composition of the CO-bearing ices by detailed comparison with laboratory spectra, or by theoretical calculation using laboratory determined optical constants. They found the $4.674 \mu\text{m}$ absorption to be due to CO mixed in with nonpolar¹ molecules such as CO_2 and O_2 or due to relatively pure CO matrices, whilst the $4.681 \mu\text{m}$ component seems to be due to CO in H_2O -dominated polar matrices. Alternatively, Palumbo & Strazzulla (1993) argued for an origin of the $4.674 \mu\text{m}$ feature in a layer of ion irradiated pure solid CO, while CO produced by ion irradiation of $\text{H}_2\text{O}:\text{CH}_3\text{OH}$ ices would be responsible for the long-wavelength component. They envisaged that there would be an inner layer of ion irradiated $\text{H}_2\text{O}:\text{CH}_3\text{OH}$ ices covered by a layer of ion irradiated pure CO, the latter evaporating if close to embedded massive YSOs. In all cases the fits to the data were reasonable, but a detailed quantitative study of the results was not presented; in particular the problems of the goodness and, more importantly, of the uniqueness of the fits were not addressed in detail. The non-uniqueness of the fit may not only hamper a conclusive identification of the mantle constituents, but also induce an incorrect estimate of the relative abundance between the nonpolar and the polar CO-ices.

Most previous work on analysing the solid-CO bands has concentrated on observations of field stars or massive YSOs, whereas here we concentrate on low mass YSOs embedded in dense cores. The CO in the environment of these low mass YSOs may be different from that in lines of sight to field stars or high mass YSOs, and may perhaps be differently affected by proximity to the YSO itself, and its radiation field. There may also be a contribution from CO in the circumstellar discs that are known to be associated with these embedded YSOs (Myers et al. 1987).

The main objective of this paper is to report observations towards deeply embedded low mass YSOs in dense cores, and to analyse the possibility of constraining the composition of the CO-bearing ices in these observed lines of sight. In future works we intend to address the implications of these results for the envelopes of the YSOs, and the fitting of the same laboratory spectra to CO absorption observed towards field stars.

¹ Polar molecules are those, such as H_2O , NH_3 , CH_3OH , H_2S etc with a significant permanent dipole moment, whereas nonpolar molecules, such as CO , CO_2 , CH_4 , O_2 have negligible moment.

2. Observations

The target sources were primarily objects included in Myers et al. (1987) which show a significant water-ice feature ($\tau_{\text{H}_2\text{O}} > 0.25$) (Sato et al. 1990, Emerson et al. in preparation), and had not been included in previous studies of solid CO. Some more evolved objects showing the characteristics of FUor stars, and already optically visible, were also included in the sample in order to monitor the effects of the evolution of the central source on the envelope. Our sample (Table 1) includes 7 Class I YSOs (in the scheme of Lada (1987)), 1 Class II, 1 EXOr, 3 FUor stars and 1 Herbig Ae Be star.

SVS12 (originally named after its discoverers (Strom et al. 1976) but also sometimes known as SSV12) is a Class I source of $\sim 20 L_\odot$ and is probably the exciting star for the Herbig-Haro object HH12 in NGC1333 (Stapelfeldt et al. 1991, Stapelfeldt 1994); it has a water ice feature with $\tau_{\text{H}_2\text{O}} = 2.9$ (Sato et al. 1990). B5 IRS1 is a Class I source of $\sim 9.6 L_\odot$ in Perseus (Fuller et al. 1991), which shows variability in the near-IR (Moore & Emerson, 1994) and has a water ice feature with $\tau_{\text{H}_2\text{O}} \simeq 1.1$ (Sato et al. 1990, Charnley et al. 1990). L1489 is a Class I source of $\sim 7 L_\odot$ which was modelled by Adams et al. (1987); it has a water ice feature with $\tau_{\text{H}_2\text{O}} = 2.9$ (Sato et al. 1990) and is associated with reflection nebulosity associated with an outflow driven cavity (Emerson & Moore 1996). L1524 is a Class I source of $\sim 1.3 L_\odot$ with a rich near IR emission line spectrum and is the lowest luminosity YSO to exhibit gaseous CO overtone bands in emission (Greene & Lada 1996). L1551NE is a Class I (or perhaps Class 0) object in Taurus discovered by Emerson et al. (1984). Its bolometric luminosity is $\sim 6 L_\odot$, it is driving an outflow (Moriarty-Schieven et al. 1995), and the derived optical extinction is ≈ 60 mag (Barsony & Chandler 1993). TMC1A is a Class I source of $\sim 2.4 L_\odot$ (Myers et al. 1987) which was modelled by Adams, Lada & Shu (1987). Its environment and outflow have been recently extensively studied by Chandler et al. (1996). Reipurth 50N is a Class I source of $\sim 250 L_\odot$ associated with reflection nebulosity and HH objects and is one of the more luminous objects in the L1641 region (Colomé et al. 1995); it has a water ice feature with $\tau_{\text{H}_2\text{O}} = 2.6$ (Casali 1991). It has been suggested that this may be an FUor type object (Strom & Strom 1993).

L1536S (L1536B in the notation of Myers et al. 1987) is a Class II source associated with optical nebulosity and has a water ice feature with $\tau_{\text{H}_2\text{O}} = 0.7$ (Sato et al. 1990).

SVS13 (originally named after its discoverers (Strom et al. 1976) but also sometimes known as SSV13) is the exciting source of the Herbig Haro chain HH7-11 in NGC1333 (Sandell et al. 1990) and underwent an EXOr type optical/infrared outburst (a scaled down FUor event) sometime between Dec 1988 and Sep 1990 (Eisloffel et al. 1991). Elias 1-12 (also known as V1735 Cyg) underwent an FUor type eruption and became visible (Kenyon & Hartmann 1991); it has a water ice feature with $\tau_{\text{H}_2\text{O}} = 0.7$ (Sato et al. 1990). FU Ori is the prototypical FUor type object (Kenyon & Hartmann 1991) and was modelled by Adams Lada & Shu (1987). ZCMA is sometimes classified as a Herbig AeBe star, but more recently has been classified as an

Table 1. Log of observations

Object	IRAS name	Type	Region	α (1950) ¹	δ (1950) ¹	UT Date
SVS12		Class I	NGC1333	03 25 55.8	+31 10 02	3/10/94
SVS13	03259+3105	EXor	NGC1333	03 25 58.2	+31 05 46	4/10/94
B5 IRS1	03445+3242	Class I	Perseus	03 44 31.8	+32 42 34	3/12/92
L1489	04016+2610	Class I	Taurus	04 01 40.6	+26 10 47	2/10/94
L1524	04239+2436	Class I	Taurus	04 23 54.5	+24 36 55	4/10/94
L1551NE		Class I	Taurus	04 28 50.5	+18 02 11	3/12/92
L1536S	04303+2240	Class II	Taurus	04 30 19.4	+22 40 17	3/12/92
TMC1A	04365+2535	Class I	Taurus	04 36 31.3	+25 35 53	3/12/92
Re50N IRS1	05380-0728	Class I	L1641	05 38 02.4	-07 29 00	3/12/92
FU Ori		FUor	Orion	05 42 37.7	+09 03 03	3/12/92
R Mon	06364+0846	HAeBe	Monoceros	06 36 26.1	+08 46 53	4/12/92
Z CMa	07013-1128	FUor	Canis Major	07 01 22.5	-11 28 36	3/12/92
Elias 1-12	21454+4718	FUor	Cygnus	21 45 26.9	+47 18 08	3/12/92

1) coordinates from telescope pointing

FUor type variable (Kenyon & Hartmann 1991) and found to be a binary (Barth et al. 1994). R Mon is a Herbig AeBe star situated at the apex of the cometary nebula NGC2261, and is associated with an IR reflection nebula and a disk (Yamashita et al 1989).

2.1. General description

Spectroscopy in the 4.5–4.9 μm window was carried out at the United Kingdom Infrared Telescope (UKIRT) at Mauna Kea in Hawaii, with the Cooled Grating Spectrometer 4 (CGS4), in the course of two observing runs: 1992 December 2,3 and 1994 October 1-4. In both runs the detector was a SBRC InSb 58×62 pixels array, and the spectra were obtained with an intermediate resolution 75 lines/mm grating. The sky subtraction employed standard chopping and nodding techniques (nodding was done along the slit so that the main and nodded spectra both appeared on the chip). A chop throw of $15''4$ was used throughout both runs, in the north-south direction in December 1992 and east-west in October 1994. All spectra were fully sampled by shifting the detector over two pixels in steps of half a pixel (2×2 sampling). The cancellation of atmospheric features was achieved by ratioing the spectrum of each object by the spectrum of a standard star observed at a similar airmass (generally within 0.1) in the same region in the sky. Flux calibration was not attempted. A log of the observations is presented in Table 1, which lists Object and IRAS name, region of sky, 1950 coordinates used, and UT date of observation.

In December 1992, the short focal length (150 mm) camera was used giving a resolving power ($\lambda/\Delta\lambda$) of ~ 760 . The slit width (one pixel) corresponded to $\sim 3''$. The wavelength scales were calibrated relative to an argon lamp, and the calibration is accurate to $\sim 0.0015 \mu\text{m}$. The weather was very unstable on both nights and most of the objects were observed through clouds, resulting in large variations of the flux level between consecutive integrations. The total integration time per object varied with the brightness of the source and with the atmospheric conditions. The useful integration time per object was typically 1 min. The useful wavelength coverage was found to be 4.58–

4.78 μm . All spectra were ratioed with the standard BS1203 (B1 I). Because a standard was not available closer than 0.3 in airmass, resulting in poor atmospheric cancellation, FU Ori was taken as a standard for Re50N IRS1 and Z CMa (FU Ori does not show evidence of any features in its spectrum).

In October 1994, the long focal length (300 mm) camera was used, and the resolving power was thus doubled to ~ 1500 and the spectral coverage was halved. The slit width (one pixel) corresponded to $\sim 1''5$. The wavelength calibration was done relative to an argon lamp and to known atmospheric absorptions present in the observed wavelength range (4.58–4.78 μm), and is accurate to $\sim 0.0005 \mu\text{m}$. Observations were made of L1489, L1524, SVS13 and SVS12. An attempt was also made to observe B5 IRS1 again (to improve the 1992 data), but it was unsuccessful as the object had faded in the M window, in agreement with the fading trend reported by Moore & Emerson (1994). The weather conditions were generally good. The typical integration time per object was 8 min. The spectra of L1489, L1524 and SVS13 were ratioed with the standard BS1543 (F6 V), and the spectrum of SVS12 was ratioed with the standard BS1131 (B1 III).

2.2. Data reduction

The data reduction was performed using the CGS4DR and FIGARO reduction packages from Starlink. For a detailed description of the data reduction procedure and of the terminology, the reader is referred to Puxley et al. (1992) and Daly (1995).

Because of the large and rapid variations of the atmosphere during the December 1992 run, the sky background was not fully removed by chopping and nodding. In an attempt to recover as much signal as possible from the sources and to obtain a good estimate of the errorbars, the following procedure was applied to each object 'group' and each standard 'group'.

First, the residual sky emission left in each nodded OBJECT-SKY pair was subtracted using POLYSKY. Then each pair was scaled to have the same flux in the central spectrum as the pair with the highest number of counts. Finally, all the pairs in each group were co-added using an iterative procedure to eliminate

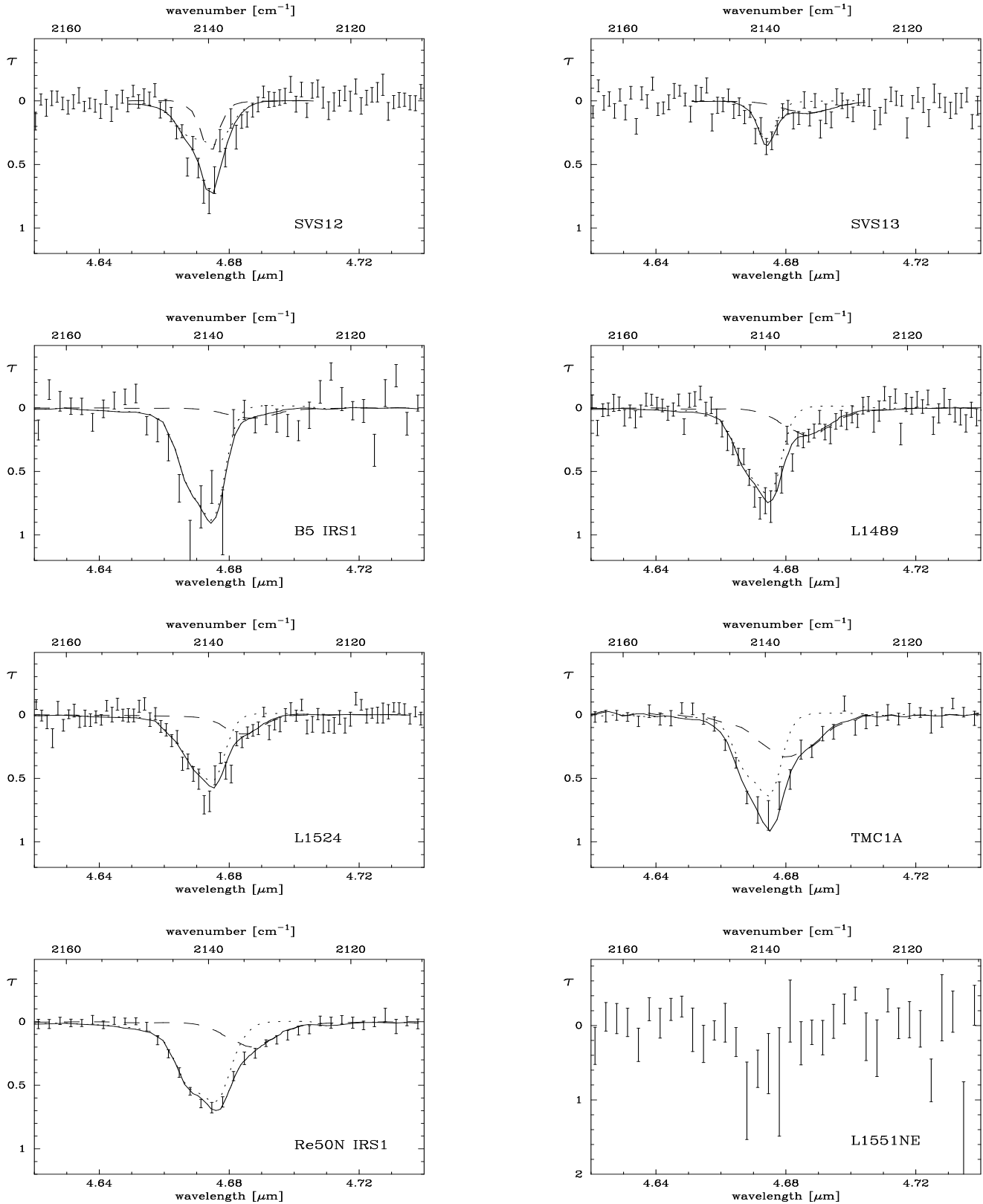


Fig. 1. Solid CO spectra of sources with CO in optical depth units, with overlaid best-matching fits. See Table 4 for composition of best fits. Dotted lines correspond to the nonpolar component, dashed lines correspond to the polar component, and solid lines to the sum of the two. An exception is made for SVS12, where the best fit corresponds to the sum of two nonpolar mixtures. The two component fitting procedure was not applied to L1551NE due to the very low S/N of its spectrum. See text for details.

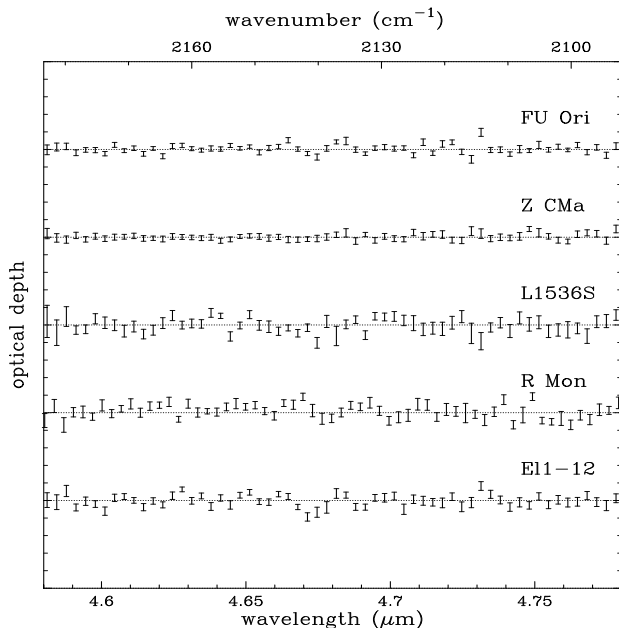


Fig. 2. Spectra of sources where only an upper limit to the solid CO feature can be placed (FU Ori, Z CMa, L1536S, R Mon) and of Elias1-12. Spectra are in optical depth units, shifted vertically by arbitrary amounts. In the y-axis, the spacing between major ticks is 1 unit in optical depth, and the spacing between minor ticks is 0.2 units. The horizontal dotted lines correspond to zero optical depth in each of the spectra.

pairs that deviated too much from the mean. The errorbars in each spectrum were estimated by calculating the standard deviation of the number of counts at each wavelength. All spectra were optimally extracted following the algorithm developed by Horne (1986) using OPTEXTRACT, and de-rippled when necessary.

As a check, this procedure was applied not only to the sources observed through clouds, but also to the few that were not affected by clouds. As expected, for the latter sources the spectra resulting from the previously described procedure were identical to those obtained with CGS4DR.

The better atmospheric stability in the October 1994 run is reflected in the data reduction, which required much less manipulation of the frames. The standard reduction procedure was carried out, using CGS4DR (it was not necessary to use POLYSKY or scaling). The spectra were optimally extracted and de-rippled when necessary.

2.3. The spectra

The final spectra, in optical depth units, are presented in Figs. 1 and 2. To determine the continua for conversion of the spectra into optical depth units, a straight line fit was performed to the points either side of the band down to $4.58 \mu\text{m}$ and up to $4.78 \mu\text{m}$, using χ^2 -minimization.

Solid CO was clearly detected in seven of the thirteen observed sources (6 out of 7 of the deeply embedded Class I ob-

Table 2. Optical depth of solid CO derived from the single component fits (L1551NE and Elias1-12), and upper limits.

Object	τ_{CO}
L1551NE	0.7 ± 0.2
Elias1-12	0.21 ± 0.04
L1536S	< 0.2
FU Ori	< 0.1
R Mon	< 0.2
ZCMa	< 0.09

jects, and the EXor): SVS12, SVS13, B5 IRS1, L1489, L1524, TMC1A and Re50N IRS1. Their spectra are presented in Fig. 1, along with the best matching laboratory mixtures (Sect. 3.1 and Table 4). At the signal to noise ratio (S/N) and resolution of the observations presented here, none of the objects shows evidence for the Pf β HI 7–5 recombination line at $\lambda = 4.6538 \mu\text{m}$ nor for the XCN absorption at $4.62 \mu\text{m}$ (Tegler et al. 1995). The P- and R-branch rovibrational lines of gas phase CO are not prominent in any of the spectra. The spectra of L1489, L1524, TMC1A and Re50N IRS1 are very similar, showing a dominant asymmetric absorption at $\sim 4.673 \mu\text{m}$ ($\sim 2140 \text{ cm}^{-1}$) with a long-wavelength wing. The absorption features in the spectra of SVS12, SVS13 and B5 IRS1 peak at approximately the same wavelength as in the other objects. However, towards these three objects the features are narrower and do not show evidence for the long-wavelength wing, although this may be due to the low S/N of the spectra.

The spectrum of the remaining deeply embedded Class I object, L1551NE (Fig. 1), shows evidence for a solid CO feature, even though each of the points near the central wavelength of the band is less than $3\text{-}\sigma$ away from the continuum. A fit to this spectrum using the fitting procedure described in Sect. 3.2 but taking one component only to fit the band, resulted in a $3.5\text{-}\sigma$ detection of a feature with an optical depth of 0.7 (Table 2). In the same way, a weak feature was identified towards the FUor Elias 1-12 (Fig. 2), with an optical depth of 0.21 ± 0.04 (Table 2). This result is in good agreement with the report of a solid CO feature with $\tau = 0.23$ towards Elias 1-12 by Tegler et al. (1995). It was not considered useful, however, to use these objects in the analysis of the solid CO band (Sect.3), because of the low S/N of the spectrum of L1551NE and the low resolution of the spectrum of Elias 1-12 compared to that of Tegler et al. (1995).

The spectra of the Class II object, L1536S, the Herbig AeBe star, R Mon, and two of the three FUors, FU Ori and ZCMa, do not show evidence of solid CO. Fig 2 shows the spectra of these sources in optical depth units. The conservative upper limits listed in Table 2 for these 4 objects were derived from the errorbars in the spectra. Although the spectrum of ZCMa does not show evidence for the Pf β emission feature detected by Tegler et al. (1995), our lack of detection is probably due to the lower resolution of the spectrum presented here.

3. Analysis of the band

As shown by several laboratory studies (e.g. Sandford et al. 1988, Schmitt et al. 1989, Palumbo & Strazzulla 1993), the spectral properties of solid state CO are affected not only by its molecular environment, structure and temperature, but also by warmup, UV irradiation and ion bombardment of the ices. Furthermore, for ices with a high concentration of CO (> 30%), particle size and shape effects, and the relative core/mantle volume also affect the profile of the band (Tielens et al. 1991).

Despite the limitations – astrophysical ices will inevitably be more complex than their laboratory analogs and astrophysical conditions cannot be properly recreated in laboratory –, it is worthwhile and useful to compare observed and laboratory features in an attempt to place constraints on the composition and structure of the astrophysical ices and on the astrophysical conditions surrounding them.

3.1. The laboratory spectra

The laboratory and computed absorption spectra used in this work for comparison with the astronomical band are listed in Table 3. Mixtures 1 to 7 (inclusive) are nonpolar or weakly polar matrices at 10 K and peak at wavelengths compatible with the shorter wavelength (4.674 μm) component of the CO-band; they will hereafter be referred to as “the nonpolar mixtures”. Mixtures 8 to 26 (inclusive) are dominated by polar molecules and peak at wavelengths compatible with the longer wavelength (4.681 μm) component of the band; they will hereafter be referred to as “the polar mixtures”.

The spectra from Tielens et al. (1991) were computed for small spherical homogeneous grains ($2\pi a \ll \lambda$, where a is the grain radius and λ is the wavelength of the incident radiation) to account for the effect of surface modes, using Mie calculations. As pointed out by Tielens et al. (1991), due to surface modes the absorption spectra of nonpolar mixtures dominated by CO (such as mixtures 2, 4 and 5, Table 3) depend considerably on the kind of particle shape or particle shape distribution assumed for the grains, as well as on the grain size distribution, on the relative core/mantle volume and indeed even on the core material. In view of the large amount of parameter space that would open up with a range of particles shapes, sizes and structures, we have, throughout this work, only considered fitting spectra for homogeneous spheres, but we note the importance of the other parameters. To get an idea of the considerable extent to which those parameters may influence the results for the CO-dominated nonpolar mixtures the spectra calculated by Tielens et al. (1991) for a variety of grains can be consulted.

The effects of warmup of the polar CO-ices are probed by mixtures 8 to 12 and 13 to 19, which correspond to H₂O:CO mixtures deposited at 10 K and subsequently warmed up to the temperature (always < 100 K) indicated in the table. Mixtures 6, 7 and 20 to 26 correspond to ices bombarded by ions and are included to probe the extent of low energy cosmic ray bombardment of the ices, or the effects of ions from flares on the YSOs. The samples were irradiated with 3 keV He ions with

stopping power similar to 1 MeV protons. The degree of irradiation is characterised by the ‘dose’ which describes the energy deposited on a grain per 16 amu equivalent atom. Doses are given here in units of eV/16amu. Finally, mixtures 20 to 26 include the presence of methanol in the matrices and the effects of warmup on irradiated ices.

It is noted that this sample of CO-bearing ices is by no means complete and should be regarded only as a starting point for the analysis of the composition of the icy grain mantles. Even though the main effects expected to affect the profile of the CO band are represented here, it should be born in mind that, before excluding any other interpretation of the profiles than that presented in this paper, a thorough analysis of all the parameters affecting the band profile should be carried out. Following studies of the composition of the CO-ices should therefore carefully explore the effects of varying particle shapes and varying irradiation doses, and the laboratory sample should be expanded to include UV and X-ray irradiation and other types of CO-bearing ices.

3.2. The fitting procedure

The fitting of the laboratory data to the observations was performed using the Marquardt method for χ^2 -minimization (Bevington 1969). For each object, the minimization routine takes the linear combination of any two laboratory spectra – $a_i S_i + a_j S_j$, $i = 1, 25$ $j = i + 1, 26$, where a_i and a_j are the amounts of the normalized laboratory spectra S_i and S_j , respectively, in optical depth units – and determines the amounts a_i and a_j that minimize the χ^2 for each pair of laboratory data. The minimization was done in the wavelength range 4.63 μm to 4.72 μm . These limits were chosen to include the whole band for all mixtures, and to allow for an average of 5 points on either side of the band for the continuum in the observations. Finally, the results of the minimization for all 325 pairs are sorted in order of increasing reduced- χ^2 (χ^2_ν) and stored in a file for later analysis.

The combination of laboratory spectra which minimizes the χ^2_ν for each of the objects is shown in Fig. 1, overlaid on the observed spectra. The results of the minimization are summarized in Table 4, where the best laboratory mixture, reduced- χ^2 and optical depths of the nonpolar and polar components are presented for each object. The χ^2_ν for the less successful mixtures will be discussed in Sect. 3.3.

The result that immediately stands out from Table 4 is that for 6 of the 7 objects, the nonpolar component of the band is best fitted by the laboratory spectrum of irradiated pure CO. The χ^2_ν values of the fits are similar for all objects except for B5 IRS1 where it is larger probably because of the relatively poor atmospheric correction of this spectrum.

The spectrum of SVS13 is best fitted by a CO:O₂ mixture, with a small contribution from a polar mixture. Indeed, the 14 best fits to the spectrum correspond to combinations of mixture no. 2 with as many polar mixtures. The next best fits, indistinguishable from these from the statistical point of view, contain predominantly mixtures no. 5 and 4. As for the polar component

Table 3. Laboratory mixtures used in the fitting procedure

Mixture no.	Mixture Content	Reference
Nonpolar mixtures (Narrow component)		
1	CO:O ₂ (2:3,10K)	Tielens et al. 1991
2	CO:O ₂ (3.8:1,10K)	"
3	CO ₂ :CO (20:1,10K)	Sandford et al. 1988
4	CO:H ₂ O (10:1,10K)	Tielens et al. 1991
5	CO (pure,10K)	"
6	CO (pure,10K), irradiated ^{2a} with 12 eV/16 amu	Palumbo & Strazzulla 1993
7	CO (pure,10K), irradiated ^{2b} with 21 eV/16 amu	"
Polar mixtures (Broad long-wavelength wing)		
8	H ₂ O:CO (4:1,10K)	Schmitt et al. 1989
9	H ₂ O:CO (4:1,25K)	"
10	H ₂ O:CO (4:1,35K)	"
11	H ₂ O:CO (4:1,50K)	"
12	H ₂ O:CO (4:1,100K)	"
13	H ₂ O:CO (20:1,10K)	Sandford et al. 1988
14	H ₂ O:CO (20:1,20K)	"
15	H ₂ O:CO (20:1,30K)	"
16	H ₂ O:CO (20:1,40K)	"
17	H ₂ O:CO (20:1,50K)	"
18	H ₂ O:CO (20:1,65K)	"
19	H ₂ O:CO (20:1,80K)	"
20	CH ₃ OH (pure, 10K), irradiated with 40 eV/16 amu	Palumbo & Strazzulla 1993
21	H ₂ O:CH ₃ OH (2:1,10K), irradiated with 27 eV/16 amu	this work ¹
22	H ₂ O:CH ₃ OH (2:1,47K), irradiated with 27 eV/16 amu	this work ¹
23	H ₂ O:CH ₃ OH (2:1,97K), irradiated with 27 eV/16 amu	this work ¹
24	H ₂ O:CH ₃ OH (2:1,10K), irradiated with 40 eV/16 amu	Palumbo & Strazzulla 1993
25	H ₂ O:CH ₃ OH (2:1,47K), irradiated with 40 eV/16 amu	this work ¹
26	H ₂ O:CH ₃ OH (2:1,67K), irradiated with 40 eV/16 amu	Palumbo & Strazzulla 1993

1. For a description of the experimental apparatus and procedure see Palumbo & Strazzulla (1993).

2. After ion-irradiation of pure CO new species are formed: **a)** CO₂ at 2346 cm⁻¹ (FWHM = 7 cm⁻¹) and suboxide at 2213 and 2244 cm⁻¹ (FWHM ~ 10 cm⁻¹); **b)** CO₂ at 2347 cm⁻¹ (FWHM = 9 cm⁻¹) and suboxide at 2211 and 2242 cm⁻¹ (FWHM ~ 10 cm⁻¹) (Strazzulla et al. 1997)

Table 4. Results of χ^2 minimization for objects with a clear CO feature

Object	Nonpolar component	$\tau_{nonpolar}$	Polar component	τ_{polar}	χ^2_{ν}
SVS12 ^a	pure CO (10K,21 <i>irru</i> ^b)	0.35 ± 0.04	CO:O ₂ (3.8:1,10K) ^a	0.41 ± 0.08	1.42
SVS13	CO:O ₂ (3.8:1,10K)	0.32 ± 0.04	H ₂ O:CO (4:1,100K)	0.10 ± 0.02	1.82
B5 IRS1	pure CO (10K,12 <i>irru</i>)	0.90 ± 0.08	H ₂ O:CO (4:1,100K)	0.08 ± 0.04	2.62
L1489	pure CO (10K,12 <i>irru</i>)	0.69 ± 0.03	H ₂ O:CO (4:1,100K)	0.22 ± 0.02	1.61
L1524	pure CO (10K,12 <i>irru</i>)	0.53 ± 0.03	H ₂ O:CO (20:1,80K)	0.15 ± 0.02	1.86
Re50N IRS1	pure CO (10K,21 <i>irru</i>)	0.64 ± 0.02	H ₂ O:CO (4:1,100K)	0.20 ± 0.02	1.11
TMC1A	pure CO (10K,12 <i>irru</i>)	0.65 ± 0.05	H ₂ O:CH ₃ OH (2:1,47K,40 <i>irru</i>)	0.33 ± 0.04	1.05

a. The best fit to the spectrum of SVS12 is obtained with two nonpolar mixtures: no.s 2 and 7. For easier comparison of the results with the other objects, mixture 7 is presented in this table as the nonpolar component and mixture 2 as the polar component of the band.

b. For convenience in the presentation of the results, an irradiation unit has been defined as: 1 *irru* = 1 eV/16 amu.

of the band, it is difficult to assess the reality of its detection, as the band is weak and the fitting routine tries to fit the wiggles in the spectrum. A (subjective) “eye-analysis” of the spectrum may argue against the existence of the polar component of the band in the spectrum of SVS13. This object will not be discussed further in this paper.

3.3. χ^2 mapping

Despite the striking similarity of the best fits for the 6 objects with the deeper CO band, it is important to assess the significance and uniqueness of such results. In particular, it is necessary to investigate how well constrained each of the components of the band is.

A convenient way to visualize the results of the fitting procedure is to produce a “ χ^2 map”: a grey-scale histogram of

the reduced- χ^2 resulting from the χ^2 -minimization for each of the 325 pairs of laboratory spectra, which was stored by the fitting routine (Sect. 3.2). An example of such a “ χ^2 map” is presented in Fig.3 for TMC1A. In this plot, the x-axis is the number assigned to each of the laboratory spectra going into the fitting routine (Table 3), the y-axis is the reduced- χ^2 , and the grey-scale is the number of counts of each mixture in χ^2_ν “bins” which are 0.1 in size. The left panel corresponds to the nonpolar mixtures and the right panel to the polar mixtures. Each pair represented in this plot contains one nonpolar mixture and one polar mixture, which produce two counts in the same χ^2 bin (i.e. row): one in the left panel for the nonpolar component and another in the right panel for the polar component. The best-matching mixture for TMC1A, for example, corresponds to the pair of mixtures 6 + 25, with a χ^2_ν of 1.05. This best fitting pair (6+25) is represented in the plot by a grey square of 1 count at (6,1.0) and another grey square of 1 count at (25,1.0). The second best-matching mixture corresponds to the pair of mixtures 6 + 19, with a χ^2_ν of 1.08. This second pair is represented in the plot by a grey square at (6,1.0) and another grey square at (19,1.0). The same is done for all other pairs and an extract, for $\chi^2_\nu < 2.6$, of the result is shown in Fig.3. Then, the grey squares at (6,1.0) and (6,1.1), for example, represent 2 and 6 counts respectively.

It is clear from this χ^2 map (Fig. 3) that the preferred mixture for the nonpolar component of the band is pure CO at 10 K irradiated with a 12 eV/16 amu dose (mixture no. 6). The mixture corresponding to pure CO at 10 K irradiated with a 21 eV/16 amu dose (mixture no. 7) also produces good fits to the spectrum. However, the choice of any other mixture for the nonpolar component results in a large increase in the reduced- χ^2 . In fact, taking into account the number of degrees of freedom in the fit, mixtures with a nonpolar component which is *not* that of irradiated pure CO can be excluded at the 97.5% confidence level.

For the polar component of the band, however, it is not possible to identify one single mixture that produces a significantly better fit than all the others. The warmed-up irradiated methanol and H₂O:CH₃OH ices (mixtures 20-26) and the highest temperature warmed-up H₂O:CO ices (mixtures 11-12 and 18-19) seem to be preferred, but amongst these it is very hard to make distinctions. In fact, the best fits ($\chi^2_\nu \leq 1.3$) are statistically similar.

The results for Re50N IRS1 show that, like for TMC1A, it is clear that irradiated pure CO is the preferred type of mixture for the nonpolar component of the band. All other nonpolar mixtures tried can be excluded at the 99% confidence level. For the polar component, irradiated methanol and H₂O:CH₃OH mixtures produce the best fits, and all H₂O:CO mixtures with less than 25% of CO fail to produce reasonable fits to the observed spectrum.

For the other objects, it is more difficult to draw definite conclusions when analysing each of them individually because of the larger values of χ^2_ν , but a coherent picture can be put together if, instead, the overall results are considered. The comparative performance of the *nonpolar* mixtures for the six objects can

readily be seen in the histogram in Fig.4, which can be thought of as overlaying the information of the seven columns in the left panel of figures such as Fig. 3. (It should be noted that the χ^2_ν results for B5 IRS1 were divided by 2 for plotting purposes.) It is clear that the best fits are *always* achieved by mixtures having irradiated pure CO as the nonpolar component (the two lightest grey bars in the right hand part of each χ^2_ν bin).

No such clear trend appears if the equivalent diagram (not shown here) is constructed for the *polar* component. In fact the analysis of all the individual objects’ χ^2 maps (not shown here except for TMC1A) shows, as was the case for that object, that it is not possible to constrain the polar component of the band. However, the 13 best fits for L1489, L1524, TMC1A and Re50N IRS1 have in common the irradiated methanol and H₂O:CH₃OH mixtures and the H₂O:CO (4:1,100 K) mixture as the polar component, combining with the irradiated pure CO as the nonpolar component. In the cases of SVS12 and B5 IRS1 the first 27 best fits correspond to the combination of irradiated pure CO with all other mixtures. That means the polar component of the CO-ices is weak or absent in these two objects, and indeed the best fit for SVS12 involves two nonpolar components (Table 4). To some extent, however, in both objects that may be due to the relatively poor atmospheric cancellation, and higher S/N observations would be needed to place further constraints on the composition of the ices in those lines-of-sight.

3.4. O₂-rich ices

One result of interest is the performance of the O₂-rich mixtures included in the laboratory sample in fitting the observed profiles. In fact, it can be seen in Fig. 4 that such mixtures (no.s 1 and 2) can generally be excluded as candidates for the nonpolar component of the ices since they provide very poor fits to the CO band. As pointed out by the referee (W. Schutte) the exclusion of mixtures where the abundance of O₂ in the ices is comparable to that of CO could have interesting implications. In particular, models of dense cloud chemistry (e.g. Tielens & Hagen 1982, d’Hendecourt et al. 1985, Bergin et al. 1995) predict that in dense regions the most abundant species in the grain mantles will be CO and O₂ in comparable amounts. However, as suggested by Schutte (1996), it may indeed be that the current models overestimate the amount of available oxygen, since the cosmic abundances generally used (derived from the solar system) seem to be overabundant in heavy elements by factors between 1.5 and 2.0 (Snow & Witt 1996).

In any case, it must be stressed that our laboratory sample only includes two O₂-rich mixtures, and that even those are computed for spherical homogeneous grains, which cannot be a good simulation of interstellar grains. The results obtained in this work cannot therefore exclude all O₂-rich ices: we are only in the position of excluding mixtures that have been included in the laboratory sample (Table 3).

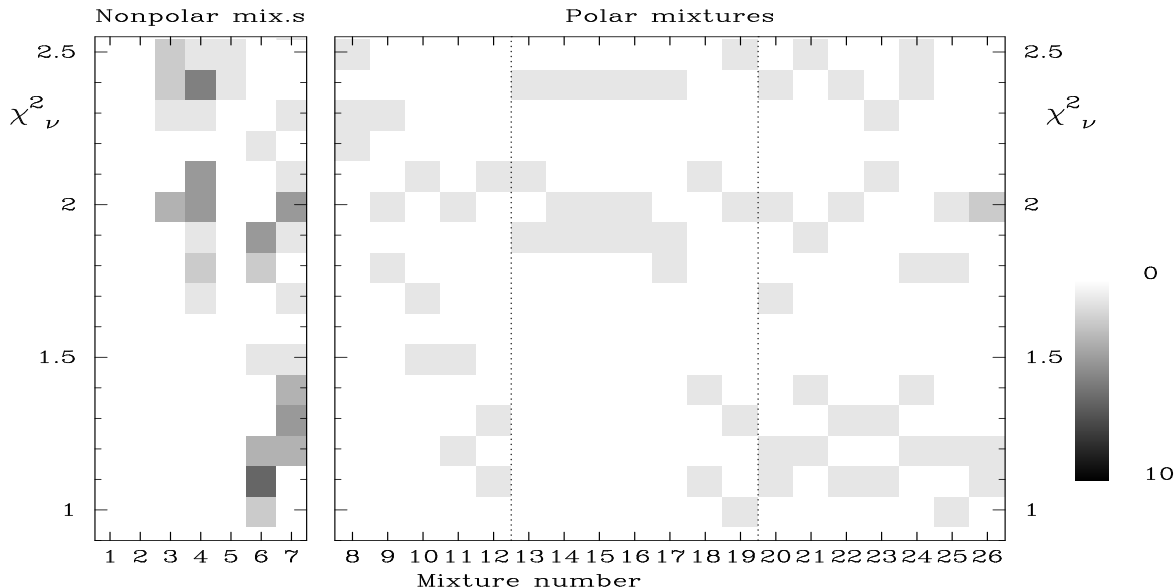


Fig. 3. χ^2 map of TMC1A. The x -axis is the mixture number identifying the laboratory spectra going into the fitting routine (Table 3); the y -axis is the reduced- χ^2 of the fits; the grey-scale is the number of counts of each mixture in χ^2_ν “bins” which are 0.1 in size. In this histogram, a χ^2_ν bin labelled k comprises values of χ^2_ν in the interval $[k, k + 0.1]$. The left panel of the plot corresponds to the results for the nonpolar mixtures and the right panel to the results for the polar mixtures. The vertical dotted lines are used as separators of polar mixtures coming from different laboratory groups.

4. Energetic processing of the ice mantles

The results of the fits presented above very strongly point to ice mantles that suffered energetic processing by ion bombardment, perhaps in the form of low energy cosmic rays or flares, or by other processes, such as X-ray or UV processing, that modify the mantle structure. There is also some evidence for warmup of some of the ices from the polar component of the band, even though less constrained. However, it should be realized that obtaining a good fit is not enough to prove the validity of a model and that reasonable physical hypotheses are needed to support it. We therefore discuss the possible astrophysical origin of the structural changes that are caused, in the laboratory situation, by ion irradiation, covering flares on the YSOs, cosmic rays and X-ray and UV processing.

4.1. Flares

All of the six sources in this work found to have a significant solid CO feature are class I embedded Young Stellar Objects and are observed to be driving molecular outflows. Recent X-ray surveys have shown that even deeply embedded young stars are X-ray emitters and indeed emit up to hard X-ray energies (Casanova et al. 1995, Koyama et al. 1994, Montmerle 1996, priv. comm.). The X-rays are possibly associated with magnetic activity, thought to be similar to solar activity but scaled up by orders of magnitude, in the form of flares or coronal mass ejection (CME) events. Since high energy particles ($E \geq 0.5$ MeV) are detected in the solar wind, in solar flares and in CMEs (Reames et al. 1996), it is likely that they will also be ejected in the winds and flares of embedded young stars. This could then account

for the ion bombardment of the icy mantles around protostellar objects. However, the flux of ions required to explain the observations might be a problem. The specific energy loss (stopping power, S) of a 1 MeV proton in a typical grain containing heavy atoms (C,N,O,Si) is $S \simeq 5 \times 10^{-15}$ eV cm²/atom (Palumbo & Strazzulla 1993). The energy deposited on a grain per equivalent 16 amu atom (the ‘dose’) by 1 MeV protons after an irradiation time Δt is given by $S \times J \times \Delta t$, where J is the proton flux. For a dose of 12 eV/16 amu, over 2×10^5 yr (the freeze-out timescale; Schutte 1996) the proton flux needed would be 380 cm⁻² s⁻¹, while over 10^8 yr (lifetime of a dark cloud; Shu et al. 1987) only 0.8 cm⁻² s⁻¹ would be required. A rough estimate of the number of protons expected from a flare in a T-Tauri star shows that the available flux may be too low. Observations have shown that pre-main sequence stars undergo flaring events which may be more than 4 or 5 orders of magnitude more energetic than solar flares. A multi-wavelength analysis of these flares supports the idea that they are solar-like, but scaled up by orders of magnitude (Gahm 1990; Haisch et al. 1991; Preibisch et al. 1995; Guenther & Emerson 1997). Moreover, Haisch et al. (1991) suggest that proton beams may carry the major fraction of the flare energy. During a typical solar flare, the energy released in \sim MeV protons is of the order of 10^{31} erg. Assuming a typical solar flare in an embedded YSO is 10^5 times more energetic than the corresponding solar one and lasts for \sim 3 hours, then the average proton flux at a representative distance² of 0.05 pc is ~ 200 cm⁻² s⁻¹. If the flaring activity in the young object

² the radius of the core where the temperature drops to 10 K and therefore where the most volatile ices can survive is roughly 0.05 pc.

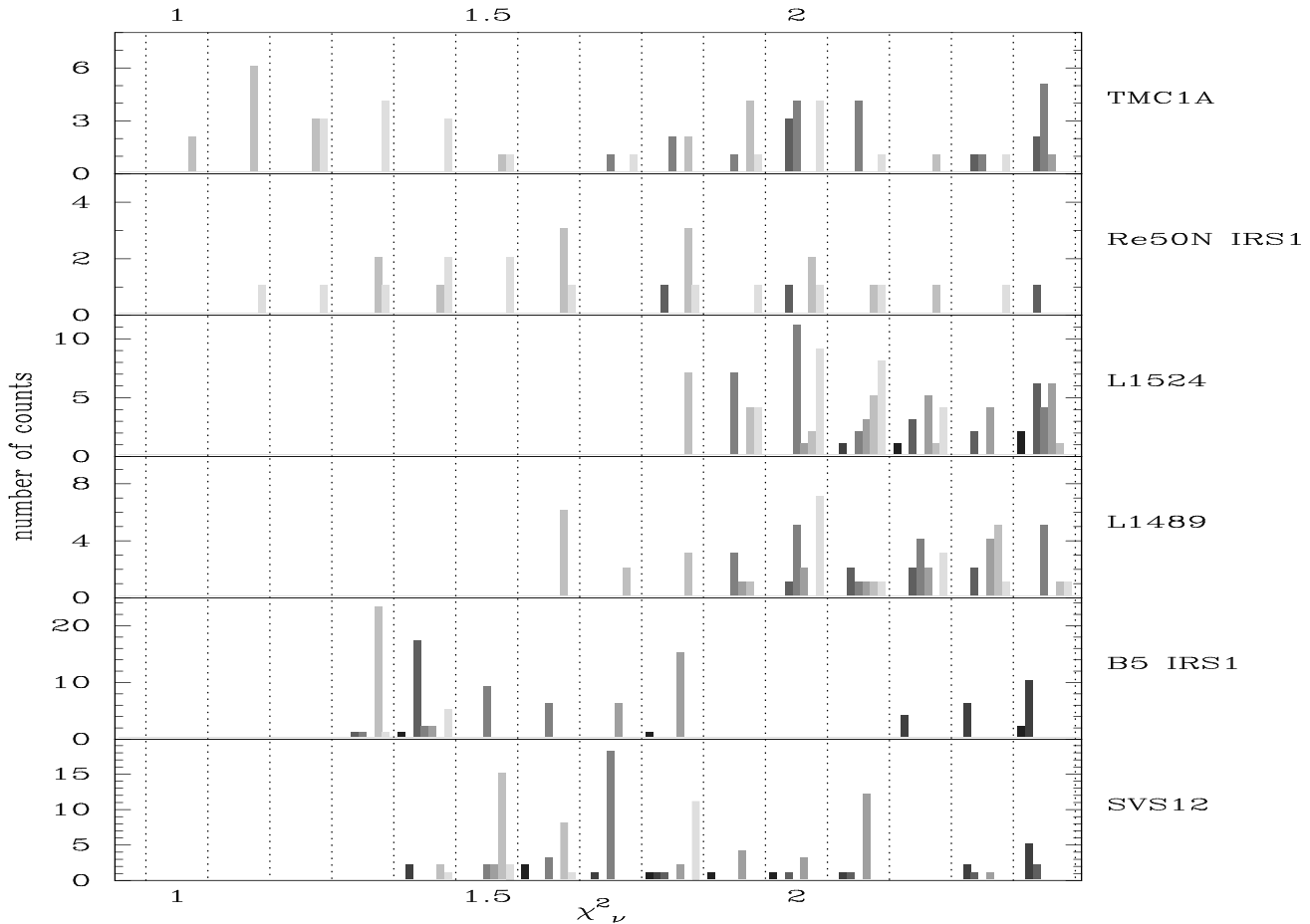


Fig. 4. Histograms of the comparative performance of the *nonpolar* mixtures, resulting from the χ^2 -minimization, for the objects showing a significant solid CO feature. The x-axis is the reduced- χ^2 of the fits in χ^2_ν “bins” which are 0.1 in size; the y-axis is the number of counts of each mixture in each χ^2_ν bin. The χ^2_ν bins are defined in the same way as in Fig.3. Within each χ^2_ν bin, the nonpolar mixtures (mixtures 1 to 7, Table 3) are represented by grey-scale bars ordered from left (mixture 1) to right (mixture 7) with decreasing intensity of the grey-scale. The χ^2_ν results for B5 IRS1 were divided by 2 to fit onto the same horizontal scale as the other objects.

maintained the proton flux constant at this level *continually*, then it would imply an irradiation time of $\sim 4 \times 10^5$ yr, which is of the order of the freeze-out timescale. However, the current statistics of flares in T-Tauri stars point to significant short-term variability during only 5% of the time (Gahm 1990; Guenther & Emerson 1997). This raises the time interval to achieve the necessary irradiation dose to $\sim 8 \times 10^6$ yr, more than one order of magnitude larger than the estimated age of class I objects ($\sim 10^5$ yr; Cabrit 1994). It may be, of course, that flaring activity is more frequent and/or more energetic in class I objects than in T-Tauri stars, but that has not been detected due to the high extinction to those objects. That could reconcile the timescale for sufficient irradiation with the age of the objects. If such a possibility is ruled out, then another source of high energy particles is required to deposit enough energy in the mantles.

4.2. Low energy cosmic rays

The flux of low energy cosmic rays ($E \sim 1$ MeV) in the interstellar medium is very uncertain. Jenniskens et al. (1993) estimate the proton flux in the diffuse medium to be $J(E \sim 1 \text{ MeV}) \simeq 0.6 - 3 \text{ cm}^{-2} \text{ s}^{-1}$. There is extensive evidence that molecular clouds are clumpy (Olano et al. 1988, Stutzki & Güsten 1990, Meixner et al. 1992, Williams et al. 1995, Langer et al. 1995). Moreover, it has been shown that interstellar UV radiation can penetrate the molecular clouds because of their clumpy structure (Howe et al. 1991, Spaans 1996). If, in the same way, low energy cosmic rays can penetrate the clouds, then the dust grains can be sufficiently irradiated provided that they can survive in a dense core *with* the CO mantles for $\sim 10^7 - 10^8$ yr. But this is also a problem: if the desorption timescale for CO ice were as long as 10^7 yr, then there would be little or no gas phase CO in dense clouds (since the freeze-out timescale is 10–100 times shorter), which is in disagreement with the observations. For this reason, low energy cosmic rays are unlikely to be a major contributor to the bombardment of the ices by high energy particles.

4.3. UV and X-ray processing

Another possibility might be, of course, that equally good fits to the observations can be obtained with laboratory samples with a smaller irradiation dose, or with other mixtures not subjected to ion bombardment. The problem with the former is that a significantly smaller irradiation dose might not broaden the CO feature sufficiently to match the observations of the nonpolar component of the band. UV or X-ray irradiation of the samples might be an alternative to ion bombardment which will be pursued in a future study. In that case, however, far out in the envelope, where the cold CO mantles are presumably abundant, there will not be a contribution to the UV flux from the embedded object, as the UV photons are not able to penetrate the thick envelope and are absorbed by the material close to the star. The UV field inside the cloud will then be responsible for the processing of the grain mantles. But if that is so, irradiated CO samples should also produce good fits to the CO features observed towards field stars. Unfortunately, the detailed studies of the solid-CO feature published so far (Kerr et al. 1993, Chiar et al. 1994, 1995) did not include irradiated CO-ices as the nonpolar component of the band. It should, however, be noticed that Palumbo & Strazzulla (1993) attempted to fit the spectra of four field stars with irradiated pure CO combined with irradiated H₂O:CH₃OH ices and obtained what looks to be good results, but because the goodness and *uniqueness* of the fits were not analysed in detail, it is difficult to draw conclusions at this stage. It is therefore vital to re-analyse the spectra of field stars observed to date including ion and UV irradiated laboratory spectra in the fitting procedure, and to study carefully the comparative performance of the different mixtures in the results and relative to the results towards embedded YSOs. Only then will it be possible to make a direct comparison between the results obtained in this work and the ones previously published by other authors.

5. Column densities

Besides the composition of the ices, it is also of great importance to determine the amount of CO frozen in the grain mantles, as it is a quantity that can be compared with the results from chemical models. The column density of solid CO in the mantles in each line-of-sight, N (molecules/cm²), can be determined from the spectra using the following expression (Sandford et al. 1988):

$$N = \frac{\int \tau_\nu d\nu}{A}$$

where τ_ν is the optical depth at wavenumber ν (cm⁻¹), and A (cm/molecule) is the integrated band absorbance (band strength).

5.1. Estimates from the best fits

The total solid CO column density for each of the sources was estimated by integrating the optical depth over the band in each spectrum. The limits of the integration varied with the extent of the band for each of the spectra. The band strength was taken

Table 5. Solid CO column densities derived from the observations, using the best fits to separate the components. Column densities given in units of 10¹⁷ molec/cm².

Object	N(CO) _{nonpolar}	N(CO) _{polar}	N(CO) _{total}
SVS12	4.0 ± 0.2	...	4.0 ± 0.2
B5 IRS1	6.5 ± 0.6	...	6.5 ± 0.6
L1489	4.3 ± 0.2	1.9 ± 0.2	6.0 ± 0.3
L1524	3.5 ± 0.2	1.3 ± 0.2	4.5 ± 0.2
Re50N IRS1	4.9 ± 0.2	1.7 ± 0.2	6.7 ± 0.2
TMC1A	3.6 ± 0.3	3.1 ± 0.4	6.9 ± 0.4

to be that of pure CO at 14 K, $A = 1.1 \times 10^{-17}$ cm/molec (Jiang et al. 1975). The resulting values for the total solid CO column density are listed in Table 5. Also presented in Table 5 are the column densities of each of the components of the band, nonpolar and polar, when both are present in the spectrum. These were estimated separately by first subtracting the laboratory spectrum corresponding to the polar (/nonpolar) component of the best fit from the spectrum, and then integrating the optical depth of the resulting band as indicated above (and adjusting the integration limits appropriately) to obtain the column density of the nonpolar (/polar) CO-ices. The band strength used was again 1.1×10^{-17} cm/molec. All the errorbars in the column densities were estimated from the errorbars in the spectra. Note that although this procedure can produce a value for $N(\text{CO})_{\text{nonpolar}} + N(\text{CO})_{\text{polar}}$ that is not equal to $N(\text{CO})_{\text{total}}$, the equality does, of course, hold within the uncertainties.

A word of caution is due at this point. The column densities derived above depend on the band strength, A , which is not well constrained. Sandford et al. (1988) and Palumbo & Strazzulla (1993) found that A could vary between 1.0×10^{-17} cm/molec for pure CO and 1.7×10^{-17} cm/molec for a CO:H₂O (1:20) mixture. However, recent laboratory simulations (Gerakines et al. 1995) only showed a 13% variation in the band strength (relative to its value for pure CO) with the composition of the mixture, and a 17% variation with the temperature. The value measured for the band strength for pure CO ice at 14 K was 1.1×10^{-17} cm/molec, and it is that value which is being adopted here for all mixtures and temperatures. This uncertainty in the value of A implies that the derived column densities, and in particular that of the polar component of the band, may not be accurate and may need to be recalculated if further laboratory work confirms a stronger dependence of A on composition and/or temperature of the mixture than that reported by Gerakines et al. (1995). However, even if that dependence is confirmed, the total column densities of solid CO reported here should only be overestimated by up to 30% by taking A constant across the feature, but probably only by as much as 10 - 20%.

5.2. Ratio of nonpolar to polar CO-ices

Apart from the uncertainty in the composition of the CO-bearing ices, the non-uniqueness of the fits to the observations also implies an uncertainty in the relative abundances of the nonpolar and polar CO-ices. To assess the extent of that problem, the

Table 6. Column densities of nonpolar and polar CO-ices, given in units of 10^{17} molec/cm².

Object		H ₂ O:CO	H ₂ O:CH ₃ OH	CH ₃ OH
L1489	χ^2_ν	1.61 ^a	1.62 ^d	1.65 ^g
	N(CO) _{np}	4.3 ± 0.2	3.3 ± 0.2	3.1 ± 0.2
	N(CO) _p	1.9 ± 0.2	2.9 ± 0.3	3.1 ± 0.2
L1524	χ^2_ν	1.86 ^b	1.86 ^e	1.86 ^g
	N(CO) _{np}	3.5 ± 0.2	3.2 ± 0.2	1.8 ± 0.2
	N(CO) _p	1.3 ± 0.2	1.5 ± 0.2	1.5 ± 0.2
Re50N	χ^2_ν	1.11 ^c	1.36 ^f	1.27 ^h
	N(CO) _{np}	4.9 ± 0.2	3.8 ± 0.2	3.6 ± 0.2
	N(CO) _p	1.7 ± 0.2	2.8 ± 0.2	3.1 ± 0.2
TMC1A	χ^2_ν	1.08 ^b	1.05 ^d	1.11 ^g
	N(CO) _{np}	4.6 ± 0.3	3.6 ± 0.3	3.4 ± 0.3
	N(CO) _p	2.0 ± 0.4	3.1 ± 0.4	3.4 ± 0.4

a. Mixtures 6 + 12. b. Mixtures 6 + 19. c. Mixtures 7 + 12.

d. Mixtures 6 + 25. e. Mixtures 6 + 26. f. Mixtures 7 + 25.

g. Mixtures 6 + 20. h. Mixtures 7 + 20.

column densities of the two components of the band were calculated separately for each object, taking 3 different fits to each spectrum which are statistically equally good. The estimated column densities were obtained for the best-matching fit having (i) a H₂O:CO mixture, (ii) an irradiated H₂O:CH₃OH mixture, (iii) irradiated pure CH₃OH as the polar component of the band. The reason for these choices will be addressed in Sect. 5.3. In all cases the nonpolar component is the irradiated pure CO because, as already explained, it always provides the best fits to the spectra. The column densities of the individual components of the band were calculated as explained in Sect. 5.1. The results can be found in Table 6 for the four objects having a significant polar component: L1489, L1524, TMC1A and Re50N IRS1.

The nonpolar to polar CO column densities ratio, $N(\text{CO})_{\text{np}}/N(\text{CO})_{\text{p}}$, depends on the choice of the fitting mixture, as can be seen in Table 6. In fact, for an H₂O:CO mixture as the polar component the ratio takes values between 2.0 and 3.0, while for CO formed by irradiation of water and methanol ices the ratio is near unity. On the other hand, because of the uncertainty of the band strength, the column density of the polar component might be underestimated by up to 50%, in which case the ratio can go up to ~ 4.0 .

Within the uncertainties there is no evidence for variation of these ratios amongst the four objects. Details of the chemistry and physics which may result in these ratios are too complex for this work to discuss, but the results are presented for possible future interpretation.

5.3. CO₂ and CH₃OH abundances

Laboratory experiments have shown that ion irradiation of CO-ice results in the production of new species in the ice (Palumbo & Strazzulla 1993). One of the main products of the irradiation is CO₂. For an irradiation dose of 12 eV/16 amu, for example, the relative abundance of CO with respect to the original species is 32% and the CO/CO₂ ratio is $\sim 12:1$. Furthermore, CO itself is readily produced by ion irradiation of water and methanol ices,

along with CO₂. The abundance of CO and CO₂ with respect to the original species after irradiation of pure methanol with a dose of 40 eV/16 amu is CH₃OH:CO:CO₂ $\sim 10:5:1$, while after irradiation of a H₂O:CH₃OH = 2:1 mixture with the same dose is H₂O:CH₃OH:CO:CO₂ $\sim 10:1:0.5:0.5$.

The abundance of solid CO₂ has always been controversial, but the first observations by ISO are now showing that CO₂ exists in all lines of sight where CO has been detected (Harwit 1996). The results of the fits described above are particularly interesting because an estimate of the abundance of CO₂ towards those objects can be made for future comparison with ISO data. The predicted CO₂ (and, see below CH₃OH) column densities are listed in Table 7. Like for CO, the calculation of the column density of CO₂ is affected by the problem of the uncertainty of the absorbance (A) of CO₂. The practical consequence of this uncertainty in the absorption strength is an uncertainty in the final composition of the laboratory mixtures after ion irradiation. For that reason, two estimates are given in Table 7 for the CO₂ column densities, using $A(\text{CO}_2) = 7.6 \times 10^{-17}$ cm/molec (Yamada & Person 1964) and $A(\text{CO}_2) = 20 \times 10^{-17}$ cm/molec (Allamandola et al. 1988). So, in the case of irradiated pure CO, for instance, adopting the lower value for A implies a CO/CO₂ ratio of 12:1, while the higher value for A implies that that ratio is 30:1. The column densities estimated here are only meant to be a lower limit to the total solid CO₂ abundance, as other processes may be operative in the production of CO₂ in the ice mantles.

The mechanism for the formation of methanol in grain mantles is uncertain. Hydrogenation of CO is a possible explanation, but laboratory experiments have shown it to be an inefficient process at low temperatures (Hiraoka et al. 1994). Another possible route is methanol formation by photolysis of formaldehyde, which is itself of uncertain origin. However, experimental simulations seem to indicate that that too is an inefficient process (Schutte et al. 1996 and references therein). Nevertheless, methanol has been observed to be an important component of the icy mantles towards luminous protostars (Allamandola et al. 1992, Schutte et al. 1996), though an upper limit of 5% on its abundance relative to water-ice has been placed in a search for methanol towards some sources in and behind the Taurus dark cloud (Chiar et al. 1996). In fact, these authors suggest that energetic processing may be necessary for methanol production by hydrogenation of CO.

Once methanol has been formed in grain mantles, it is rapidly destroyed by photons and/or ion/low energy cosmic-ray bombardment to reform CO, as shown by laboratory experiments of ion bombardment of methanol containing ices (Palumbo & Strazzulla 1993) and of UV irradiation of pure ices (Gerakines et al. 1996). The results obtained in the fits to the spectra presented in this work seem to indicate that this mechanism might be responsible for the observed polar CO ices. In that case, it is possible to estimate the amount of methanol that should be present in the water-dominated ices towards the sources being studied here. The methanol column densities predicted from the best fits containing irradiated methanol ices are given in Table 7. If this route for CO formation in polar ices is

Table 7. Predicted column densities (molec/cm²) for CH₃OH and CO₂

Object	N(CH ₃ OH)	A(CO ₂) = 7.6 × 10 ⁻¹⁷ cm/molec			A(CO ₂) = 20 × 10 ⁻¹⁷ cm/molec		
		N(CO ₂) _{np}	N(CO ₂) _p	N(CO ₂) _{total}	N(CO ₂) _{np}	N(CO ₂) _p	N(CO ₂) _{total}
nonpolar component: CO + 12 eV/16 amu; polar component: H ₂ O:CH ₃ OH = 2:1 + 40 eV/16 amu							
L1489	5.8 × 10 ¹⁷	2.7 × 10 ¹⁶	2.9 × 10 ¹⁷	3.2 × 10 ¹⁷	1.1 × 10 ¹⁶	1.2 × 10 ¹⁷	1.3 × 10 ¹⁷
L1524	3.0 × 10 ¹⁷	2.6 × 10 ¹⁶	1.5 × 10 ¹⁷	1.8 × 10 ¹⁷	1.1 × 10 ¹⁶	6.0 × 10 ¹⁶	7.0 × 10 ¹⁶
Re50N IRS1 ^a	5.6 × 10 ¹⁷	3.2 × 10 ¹⁶	2.8 × 10 ¹⁷	3.1 × 10 ¹⁷	1.3 × 10 ¹⁶	1.1 × 10 ¹⁷	1.2 × 10 ¹⁷
TMC1A	6.2 × 10 ¹⁷	3.0 × 10 ¹⁶	3.1 × 10 ¹⁷	3.4 × 10 ¹⁷	1.2 × 10 ¹⁶	1.2 × 10 ¹⁷	1.3 × 10 ¹⁷
nonpolar component: CO + 12 eV/16 amu; polar component: CH ₃ OH + 40 eV/16 amu							
L1489	6.2 × 10 ¹⁷	2.6 × 10 ¹⁶	6.2 × 10 ¹⁶	8.8 × 10 ¹⁶	1.0 × 10 ¹⁶	2.1 × 10 ¹⁶	3.1 × 10 ¹⁶
L1524	3.0 × 10 ¹⁷	1.5 × 10 ¹⁶	3.0 × 10 ¹⁶	4.5 × 10 ¹⁶	6.0 × 10 ¹⁵	1.0 × 10 ¹⁶	1.6 × 10 ¹⁶
Re50N IRS1 ^a	6.2 × 10 ¹⁷	3.0 × 10 ¹⁶	6.2 × 10 ¹⁶	9.2 × 10 ¹⁶	1.2 × 10 ¹⁶	2.1 × 10 ¹⁶	3.3 × 10 ¹⁶
TMC1A	6.8 × 10 ¹⁷	2.8 × 10 ¹⁶	6.8 × 10 ¹⁶	9.6 × 10 ¹⁶	1.1 × 10 ¹⁶	2.3 × 10 ¹⁶	3.4 × 10 ¹⁶

a. For this object the nonpolar component is CO + 21 eV/16 amu.

taking place in the circumstellar envelopes of these protostars, then the abundance of methanol in the grain mantles should be comparable to the abundance of solid CO in the same lines-of-sight, and should therefore be detectable by spectroscopy of the infrared bands of methanol.

It is therefore important to carry out a search for solid methanol towards those objects, to help discriminate between the different mixtures that produce equally good fits to the solid CO spectra. That would shed light on the origin of the polar component of the CO-ices, and on the mechanism of formation and fate of methanol in grain mantles.

6. Conclusions

Observations of the solid-CO feature at 4.67 μm (2140 cm⁻¹) have been presented towards low mass YSOs in nearby molecular clouds (mostly towards deeply embedded Class I objects in the Taurus region). A detailed study of the feature by comparison of the observed spectra with the spectra of laboratory astrophysical ice analogs shows that ion irradiated ices produce excellent fits to the observations. In particular the nonpolar component of the band seems to be well constrained within the (limited) laboratory sample of CO-ices used in this work, and corresponds to irradiated pure CO for all the objects with a significant CO feature. From the statistical point of view, it is not possible to constrain the composition of the polar component of the band, although irradiated and warmed-up ices seem to be preferred. However, if the nonpolar CO-ices suffer energetic processing by ion bombardment, it is only reasonable to expect that the polar CO-ices will be processed in the same way, since CO-dominated ices accrete on top of the H₂O-dominated mantle where CO molecules may be trapped.

As a result of the ion bombardment of the ice mantles new species are formed, which could be searched for and give information on the processes suffered by interstellar ices and on the composition of the nonpolar component. In fact, suboxides are formed (Table 3) upon irradiation of pure CO samples which are not formed after irradiation of O₂-rich mixtures, while ozone (at 1040 cm⁻¹, FWHM = 10 cm⁻¹) is formed in the latter case but not in the former. In both cases CO₂ is formed, but the

resulting band is narrower and peaks at a longer wavenumber after irradiation of pure CO (2346 cm⁻¹, FWHM = 7 cm⁻¹) than after irradiation of O₂-rich mixtures (2344 cm⁻¹, FWHM = 12 cm⁻¹).

The origin of the ion irradiation is not clear. One possibility is that it may be due to high energy particles accelerated in flares, CME events and winds from the embedded YSO. If the clouds are clumpy enough to allow the penetration of a sufficient flux of low energy cosmic-rays, X-rays or UV radiation deep into the cloud, then the structural changes of the icy mantles may be due to a combination of cosmic-ray bombardment and UV and X-ray irradiation. To discriminate between these possibilities, it is important to re-analyse in detail the published solid CO observations, and compare the results towards embedded YSOs and towards field stars. It is also very important to expand the sample of laboratory spectra to contain the effects of varying particle shapes, varying irradiation doses, of UV and X-ray irradiation, and to include new types of CO-bearing matrices. In view of the goodness of the fits obtained in this work, the results are meant to be a *possibility* for the composition of the CO ices in the grains, although other possibilities should *not* be excluded. The problem of the composition of the ices will be very hard to settle definitely.

The solid-CO column densities were estimated from the spectra. It was shown that the abundance ratio of nonpolar to polar CO ices is dependent on the choice of fit to the CO feature and on the value of the strength of the band. However, there is no evidence for the variation of this ratio amongst the objects analysed in this work.

Finally, the predicted abundance of solid CO₂ and solid CH₃OH were estimated from the solid CO results. The solid CO₂ abundances predicted here are comparable to the solid CO abundances, which is in excellent agreement with preliminary reports of the ISO observations of solid CO₂ towards several lines of sight. The predicted solid methanol column densities for the 4 objects analysed here are one order of magnitude higher than the upper limits recently placed towards other lines of sight in Taurus and should therefore be detectable towards the objects discussed in this paper. It is important to carry out a search for solid methanol towards these objects, to confirm or rule out the

existence of methanol-rich mantles in the grains, and to shed light on the understanding of the origin and fate not only of methanol itself, but of the simplest but so important constituent of the ices: CO.

Acknowledgements. We thank the referee, Willem Schutte, for the very helpful comments and suggestions, which resulted in an improved version of the paper. Tom Kerr is gratefully acknowledged for providing digitized versions of the laboratory mixtures 1 to 5 and 8 to 19. We thank A. Claudio Castorina for help in taking some of the laboratory spectra presented here. TCT wishes to thank Andy Adamson for useful advice on the data reduction, the JACH for providing accommodation, and the staff at the JACH for all the discussions and friendliness during the stay there. The United Kingdom Infrared Telescope is operated by the Observatories on behalf of the UK Particle Physics and Astronomy Research Council. We acknowledge use of Starlink hardware and software in our data analysis. TCT supported by grants CIENCIA/BD/2095/92-RM and PRAXIS XXI/BD/5622/95 from JNICT, Portugal.

References

- Adams F.C., Lada C.J., Shu F.H., 1987, *ApJ*, 312, 788
 Allamandola L.J., Sandford S.A., Tielens A.G.G.M., Herbst T.M., 1992, *ApJ*, 399, 134
 Allamandola L.J., Sandford S.A., Valero G.J., 1988, *Icarus*, 76, 225
 Barsony M., Chandler C.J., 1993, *ApJ*, 406, L71
 Barth W., Weigelt G., Zinnecker H., 1994, *A&A*, 291, 500
 Bergin E.A., Langer W.D., Goldsmith P.F., 1995, *ApJ*, 441, 222
 Bevington P.R., 1969, *Data Reduction and Error Analysis for the Physical Sciences*, McGraw-Hill
 Cabrit S., 1994, in *Star Formation and Techniques in Infrared and mm-Wave Astronomy*, eds T.P. Ray and S.V.W. Beckwith, p.1
 Casali M., 1991, *MNRAS*, 248, 229
 Casanova S., Montmerle T., Feigelson E.D., Andre P., 1995, *ApJ*, 439, 752
 Chandler C.J., Terebey S., Barsony M., Moore T.J.T., Gautier T.N., 1996, *ApJ*, 471, 308
 Charney S.B., Whittet D.C.B., Williams D.A., 1990, *MNRAS* 245, 161
 Chiar J.E., Adamson A.J., Kerr T.H., Whittet, D.C.B., 1994, *ApJ*, 426, 240
 Chiar J.E., Adamson A.J., Kerr T.H., Whittet, D.C.B., 1995, *ApJ*, 455, 234
 Chiar J.E., Adamson A.J., Whittet, D.C.B., 1996, *ApJ*, 472, 665
 Colomé C., di Francesco J., Harvey P.M., 1996, *ApJ*, 461, 909
 Daly P.N., 1995, *Starlink User Note 27*, Starlink Project, CCLRC
 de Graauw Th., Whittet D.C.B., Gerakines P.A., et al., 1996, *A&A*, 315, L345
 Eiroa C., Hodapp K.W., 1989, *A&A*, 210, 345
 Eislöffler J., Guenther E., Hessman F.V., et al., 1991, *ApJ*, 383, 219
 Emerson J.P., Harris S., Jennings R.E., et al., 1984, *ApJ*, 278, L49
 Emerson J.P., Moore T.J.T., 1996, in *Polarimetry of the Interstellar Medium*, eds W.G. Roberge and D.C.B. Whittet, ASP Conference Series, 97, 350
 Fuller G.A., Myers P.C., Welch W.J., et al., 1991, *ApJ*, 376, 135
 Gahm G.F., 1990, in *Flare Stars in Star Clusters, Associations and the Solar Vicinity*, IAU Symposium 137, eds Mirzoyan, L.V., Pettersen, Tsvetkov, M.K., Kluwer, p.193
 Gerakines P.A., Schutte W.A., Greenberg J.M., van Dishoeck E.F., 1995, *A&A*, 296, 810
 Gerakines P.A., Schutte W.A., Ehrenfreund P., 1996, *A&A*, 312, 289
 Greene T.P., Lada C.J., 1996, *ApJ*, 461, 345
 Grim R.J.A., Baas F., Geballe T.R., Greenberg J.M., Schutte W., 1991, *A&A*, 243, 473
 Guenther E.W., Emerson J.P., 1997, *A&A*, 321, 803
 Gürtler J., Henning Th., Kömpe C., et al., 1996, *A&A*, 315, L189
 Haisch B., Strong K.T., Rodonò M., 1991, *ARA&A*, 29, 275
 Harwit M., 1996, *ISO Info* 9, 2
 d'Hendecourt L.B., de Muizon M.J., 1989, *A&A*, 223, L5
 d'Hendecourt L.B., Allamandola L.J., Greenberg J.M., 1985, *A&A*, 152, 130
 Hiraoka K., Ohashi N., Kilhare Y., Yamamoto K., Yamashita A., 1994, *Chem. Phys. Lett.*, 229, 408
 Horne K., 1986, *PASP*, 98, 609
 Howe J.E., Jaffe D.T., Genzel R., Stacey G.J., 1991, *ApJ*, 373, 158
 Jenniskens P., Baratta G.A., Kouchi A., et al., 1993, *A&A*, 273, 583
 Jiang G.J., Person W.B., Brown K.G., 1975, *J. Chem. Phys.*, 64, 1201
 Kenyon, S.J., Hartmann L.W., 1991, *ApJ*, 383, 664
 Kerr T.H., Adamson A.J., Whittet D.C.B., 1993, *MNRAS*, 262, 1047
 Koyama K., Maeda Y., Ozaki M., et al., 1994, *PASJ*, 46, L125
 Lada C.J., 1987, in *Star Forming Regions*, eds M. Peimbert and J. Jugaku (Dordrecht:Reidel), p.1
 Langer W.D., Velusamy T., Kuiper T.B.H., et al., 1995, *ApJ*, 453, 293
 Leto G., Palumbo M.E., Strazzulla G., 1996, *Nuc. Instr. and Meth. in Phys. Res. section B*, 116, 49
 Meixner M., Haas M.R., Tielens A.G.G.M., et al., 1992, *ApJ*, 390, 499
 Moore T., Emerson J.P., 1994, *MNRAS*, 271, 243
 Moriarty-Schieven G.H., Butner H.M., Wannier P.G., 1995, *ApJ*, 445, L55
 Myers P.C., Fuller G.A., Mathieu R., et al., 1987, *ApJ*, 319, 340
 Olano C.A., Walmsley C.M., Wilson T.L., 1988, *A&A*, 196, 194
 Palumbo M.E., Strazzulla G., 1993, *A&A*, 269, 568
 Preibisch Th., Neuhäuser R., Alcalá J.M., 1995, *A&A*, 304, L13
 Puxley P.J., Beard S.M., Ramsay S.K., 1992, *Proceedings of 4th ESO/ST-ECF Data Analysis Workshop*, ed P. Grosbald
 Reames D.V., Barbier L.M., Ng C.K., 1996, *ApJ*, 466, 473
 Sandell G., Aspin C., Duncan W.D., Robson E.I., Dent W.R.F., 1990, *A&A*, 232, 347
 Sandford S.A., Allamandola L.J., Tielens A.G.G.M., Valero L.J., 1988, *ApJ*, 329, 498
 Sato S., Nagata T., Tanaka M., Yamamoto T., 1990, *ApJ*, 359, 192
 Schmitt B., Greenberg J.M., Grim R.J.A., 1989, *ApJ*, 340, L33
 Schutte W.A., 1996, in *The Cosmic Dust Connection*, ed. J.M. Greenberg, Kluwer Academic Publishers, 1
 Schutte W.A., Gerakines P.A., Geballe T.R., van Dishoeck E.F., Greenberg J.M., 1996, *A&A*, 309, 633
 Shu F.H., Adams F.C., Lizano S., 1987, *ARA&A*, 25, 23
 Skinner C.J., Tielens A.G.G.M., Barlow M.J., Justannont K., 1992, *ApJ*, 399, L79
 Snow T.P., Witt A.N., 1996, *ApJ*, 468, L65
 Spaans M., 1996, *A&A*, 307, 271
 Stapelfeldt K.R., 1994, in *Astronomy with Millimeter and Submillimeter Wave Interferometry*, eds M. Ishiguro and W.J. Welch, ASP Conference Series, 59, 270
 Stapelfeldt K.R., Beichman C.A., Hester J.J., Scoville N.Z., Gautier T.N., 1991, *ApJ*, 371, 226
 Strazzulla G., Brucato J.R., Palumbo M.E., Satorre M.A., 1997, *A&A*, 321, 618
 Strom S.E., Vrba F.J., Strom K.M., 1976, *AJ*, 81, 314
 Strom K.M., Strom S.E., 1993, *ApJ*, 412, L63
 Stutzki J., Güsten R., 1990, *ApJ*, 356, 513
 Tanaka M., Sato S., Nagata T., 1990, *ApJ*, 352, 724

- Tanaka M., Nagata T., Sato S., Yamamoto T. 1994, ApJ, 430, 779
- Tegler S.C., Weintraub D.A., Rettig T.W., et al., 1995, ApJ, 439, 279
- Tielens A.G.G.M., Allamandola L.J., 1987, in Physical processes in interstellar clouds, eds. G.E. Morfill and M. Scholer, Kluwer, p.333
- Tielens A.G.G.M., Hagen W., 1982, A&A, 114, 245
- Tielens A.G.G.M., Tokunaga A.T., Geballe T.R., Baas F., 1991, ApJ, 381, 181
- Whittet D.C.B., 1993, in Dust and chemistry in Astronomy, eds T.J. Millar and D.A. Williams, IOP Publ. Ltd., Bristol, p.1
- Whittet D.C.B., Bode M.F., Longmore A.J., Adamson A.J., McFadzean A.D., 1988, MNRAS, 233, 321
- Whittet D.C.B., Duley, W.W., 1991, A&A Review, 2, 167
- Williams J., Blitz L., Stark A.A., 1995, ApJ, 451, 252
- Yamada H., Person W.B., 1964, J.Chem.Phys., 41, 2478
- Yamashita T., Sato S., Nagata T., et al., 1989, ApJ, 832, 837